Article ID: 1006-8775(2012) 04-0457-16

STATISTIC CHARACTERISTICS OF MCSS OVER ASIA AND WESTERN PACIFIC REGION

SHU Yu (束　宇)[1, 2], PAN Yi-nong (潘益农)[1], WANG Wei (王　微)[1]

(1. School of Atmospheric Sciences and Key Laboratory for Mesoscale of Severe Weather / Ministry of Education, Nanjing University, Nanjing 210093 China; 2. Nanjing Meteorology Bureau, Nanjing 210008 China)

Abstract: Mesoscale convective systems (MCSs) are severe disaster-producing weather systems. Previous attempts of MCS census are made by examining infrared satellite imageries artificially, with subjectivity involved in the process unavoidably. This method is also inefficient and time-consuming. The disadvantages make it impossible to do MCS census over Asia and western Pacific region (AWPR) with an extended span of time, which is not favorable for gaining a deeper insight into these systems. In this paper, a fire-new automatic MCS identification (AMI) method is used to capture four categories of MCSs with different sizes and shapes from numerical satellite infrared data. 47,468 MCSs are identified over Asia and western Pacific region during the warm season (May to October) from 1995 to 2008. Based on this database, MCS characteristics such as shape, size, duration, velocity, geographical distribution, intermonthly variation, and lifecycle are studied. Results indicate that the number of linear MCSs is 2.5 times that of circular MCSs. The former is of a larger size while the latter is of a longer duration. The 500 hPa steering flow plays an important role in the MCS movement. MCSs tend to move faster after they reach the maximum extent. Four categories of MCS have similar characteristics of geographical distribution and intermonthly variation. Basically, MCSs are zonally distributed, with three zones weakening from south to north. The intermonthly variation of MCSs is related to the seasonal adjustment of the large-scale circulation. As to the MCSs over China, they have different lifecycle characteristics over different areas. MCSs over plateaus and hill areas, with only one peak in their lifecycle curves, tend to form in the afternoon, mature at nightfall, and dissipate at night. On the other hand, MCSs over plains, which have several peaks in their lifecycle curves, may form either in the afternoon or at night, whereas MCSs over the oceans tend to form at midnight. Affected by the sea-land breeze circulation, MCSs over coastal areas of Guangdong and Guangxi always come into being at about 1500 or 1600 (local time), while MCSs over the Sichuan Basin, affected by the mountain-valley breeze circulation, generally initiate nocturnally.

Key words: mesoscale convective systems; automatic MCS identification (AMI) method; velocity; geographical distribution; intermonthly variation; lifecycle

CLC number: P458.2 **Document code:** A

1 INTRODUCTION

Mesoscale convective systems (MCSs) can cause various convective weather, such as tornado, hailstone, gale and lightning[1, 2]. Additionally, MCSs may produce heavy rain in a broad range[3]. Especially, mesoscale convective complex (MCC) and persistent elongated convective system (PECS), two special types of MCS, could bring about disastrous rainstorms and flood[4]. Given the profound influence MCSs have on Asia and western Pacific region (AWPR), continued study is essential in gaining a deeper insight into these systems.

MCSs, with small temporal-spatial scales, often take place in the evening and night. Hence, satellite and radar data with high temporal-spatial resolution are powerful tools for MCS surveillance. Satellites could be used to get a whole cognition of MCS[5, 6, 7, 8], while radar data would benefit further understanding of the details about convective activities under the cloud shield[2, 4, 9, 10, 11].

Since Maddox[5] first classified a particular type of MCSs by means of infrared satellite imageries, researchers have performed several studies on MCS census. Previous studies succeeded in deepening our insights of MCSs. However, they were always

Received 2011-02-25; **Revised** 2012-08-21; **Accepted** 2012-10-15
Foundation item: National Natural Science Founds of China (40875028); Project Funded by the Priority Academic Program Development of Jiangsu Higher Education Institutions
Biography: SHU Yu, engineer, primarily undertaking research on mesoscale meteorology.
Corresponding author: Pan Yi-nong, e-mail: pyn@nju.edu.cn

confined to either a relatively small space and time frame, or a particular type of MCSs. The main cause of these limitations is the method used in the MCS census. When identifying MCS from infrared satellite imageries, researchers need to analyze every nephogram in order to find the potential MCS. Thus, the inefficient process will waste immense manpower and time and bring about unavoidable subjectivity. In fact, computer can perform the work perfectly instead of human. In this paper, a brand-new automatic identification method[12] is used to investigate four categories of MCSs with different sizes and shapes over AWPR during the warm seasons (May to October) of 1995–2008.

Relevant observational MCS studies done in the past and the MCS definitions used in the present study are discussed and defined respectively in section 2. Section 3 provides an overview of the data and method. The results of the investigation and basic characteristics of each MCS category are presented in section 4. In addition, this section provides further analysis of MCS characteristics of the velocity, geographical distribution, intermonthly variation, and lifecycle. Finally, section 5 provides a summary and conclusions.

2 BACKGROUND

Several MCS studies have attempted to classify MCSs into discrete categories by a variety of different methods and perspectives. The most common perspectives of MCS classification have involved analyzing satellite characteristics of the systems. Similar to previous studies, the present study attempts to classify MCSs by satellite characteristics; however, unlike previous studies, the fire-new automatic MCS identification (AMI) method is used in this study instead of manual work. Therefore, the present study is able to investigate MCSs in a large temporal and space frame, which favors gaining a deeper insight into MCS climatic characteristics and regional differences. Several studies on the classification of MCSs by satellite characteristics have emerged in the past 30 years, and the most influential studies are discussed in the following subsections.

2.1 *Satellite survey of MCSs*

Maddox[5] first classified a particular type of MCSs by means of satellite imageries, and termed these well-organized, quasi-circular, meso-α[13] convective weather systems MCCs. Augustine and Howard[14] proposed to remove the ≤–32°C size requirement of the cloud shield from Maddox's original definition of MCCs in order to simplify the identification and documentation procedure. It is noteworthy to mention that Cotton et al.[8] set forth an alternative dynamical definition of MCCs, which relates the horizontal scale of MCCs to the Rossby radius of deformation. Augustine and Howard[14, 15] examined in detail the MCCs over United States during 1985–1987 and got basic understanding of MCC activities in North America. Velasco and Fritsch[16], Miller and Fritsch[17], Laing and Fritsch[18, 19] performed investigations into MCC activities in America south of 20°N, west Pacific, Indian subcontinent and Africa, respectively. In these studies, they analyzed the characteristics of the MCCs, and pointed out that MCCs—always forming on the leeward sides of megarelief—generally take place over the continents and during the night.

Another large class of MCSs, persistent elongated convective system (PECS), was defined by Anderson and Arritt[20]. PECSs are what might be considered the "linear" version of MCCs, as the only difference between a PECS and a MCC is the shape of the system. PECSs have eccentricities between 0.2 and 0.7 while MCCs must have eccentricities ≥0.7. Ma et al.[21] termed two circular MCS categories MαCS (Meso-α Convective System) and MβCS (Meso-β Convective System), respectively. Furthermore, they surveyed the MαCSs and MβCSs over China and its adjacent areas during 1993–1995 and uncovered the characteristics of temporal and spatial distributions of the MCSs. It is noteworthy to mention that Jirak et al.[4] classified MCSs over United States during 1996–1998 into four discrete categories by means of both satellite data and radar data. In their studies, the environment, severe weather and life cycles of each MCS category were also analyzed. Besides, based on the TRMM (Tropical Rainfall Measuring Mission) satellite, Romatschke and Houze[22] studied on the precipitating convective systems in South Asia monsoon area.

In the studies mentioned above, the artificial identification method was used to capture MCSs from infrared satellite imageries. Therefore, the identifying processes were somewhat subjective. To avoid this disadvantage, an alternative method was used to inquire the MCSs over China during 1996–2006 by Zheng et al.[23]. In their studies, they analyzed the local MCS activity frequency instead of capturing MCSs. Somewhere and sometime, if the cloud top temperature was lower than –52°C, the number of MCS activities in that place would increase by one. This improved method, which is based on Eulerian viewpoint, well avoids the embarrassments coming from the artificial identification method, such as the problem of subjectivity and the limitation of being unable to investigate plentiful MCS samples. But, they got in trouble when analyzing the lifecycle and movement of MCSs. What's worse, many non-MCS systems, such as tropical cyclones (TCs) and some upper cirruses, the cloud top temperature of which were also lower than –52°C, were included during

identification of MCSs; therefore, the accuracy of the final results decreased.

Different from the past artificial identification method, Shu and Pan[12] developed an AMI method by means of infrared satellite imageries. This new method can greatly reduce the consumed manpower and time, and eliminate the subjectivity arising from the identifying process. Compared with the method used by Zheng et al.[23] which is based on Eulerian viewpoint, the AMI method which is based on Lagrange viewpoint can catch the whole MCS lifecycle from formation to withering away. Hence, it is possible to investigate MCSs of various categories and to study the MCS characteristics of lifecycle and movement. In this paper, under such background, four MCS categories with different sizes and shapes are investigated over AWPR during the warm seasons of 1995–2008 by the AMI method; furthermore, characteristics of the MCSs are analyzed.

2.2 *MCS categories and terminology*

Similar to the study made by Jirak et al.[4], the present study attempts to classify MCSs into four discrete categories according to their sizes and shapes (Table 1): MαCCS (Meso-α Circular Convective System), MαECS (Meso-α Elongated Convective System), MβCCS (Meso-β Circular Convective System) and MβECS (Meso-β Elongated Convective System). In Table 1, the 50000 km^2 and 30000 km^2 size criterions are followed from Jirak's definitions of meso-α and meso-β systems, respectively. In order to make the definition of circular MCS keep up with the previous studies in China, 0.5 is chosen as the eccentricity criterion to distinguish between circular and linear MCSs. Besides, MαCCS and MαECS are used to term the meso-α systems so that they would not be confused with MCC and PECS, and the four categories of MCSs may have similar names.

Table 1. MCS definitions that are based on analysis of IR satellite data.

MCS category	Size	Duration	Shape
MαCCS	Cold cloud region ≤ –52°C with area ≥ 50000 km^2	Size definition met for ≥3h	Eccentricity ≥ 0.5 at time of maximum extent
MαECS			0.2 ≤ Eccentricity < 0.5 at time of maximum extent
MβCCS	Cold cloud region ≤–52°C with area ≥30000 km^2 and maximum size must be ≥50000 km^2		Eccentricity ≥ 0.5 at time of maximum extent
MβECS			0.2 ≤ Eccentricity < 0.5 at time of maximum extent

As discussed in Parker and Johnson[11], the appropriate MCS timescale is f^{-1}, which is approximately 3 h for the midlatitudes. Using an advection assumption, we define the MCS time scale as T = L/U. According to the definitions in Table 1, the length scales (L) of the meso-α and meso-β systems are about 126 km and 97 km, respectively. Then, an average midlatitude wind speed (U) of 10 m s^{-1} yields a MCS time scale of 3 h. Hence, the duration criterion for all the MCSs in this study is set at ≥ 3 h. As a result, the definitions of MαCCS and MαECS are different from the classical definitions of MCC and PECS in both the eccentricity criterion and the duration criterion.

In following sections, for convenience of expression, MαCCS and MαECS are collectively referred to as MαCS, while MβCCS and MβECS are collectively called by MβCS. Similarly, MαCCS and MβCCS are collectively referred to as MCCS (Mesoscale Circular Convective System), whereas MαECS and MβECS are collectively called MECS (Mesoscale Elongated Convective System). Formation time of MCS is defined as the time when the size criterion is firstly satisfied. Maturation is the time when the cold cloud shield reaches the maximum extent. Dissipation is the time when the size criterion will be no longer satisfied. Duration is defined as the lasting time from formation to dissipation.

3 DATA AND AUTOMATIC MCS IDENTIFICATION METHOD

One goal of this study was to sample a large number of MCSs from infrared satellite imageries; thus, the software Satellite Image and MCS Plot, which is based on the AMI method, was used to search and record MCSs. Based on previous MCS studies, the range of May through October seemed to be an appropriate time frame to study the active convective season of AWPR. Furthermore, a 14-yr period from 1995 to 2008 was selected to obtain a large and varied sample of MCSs so that the climatic characteristics of MCSs may be analyzed from this large MCS database. During this period, any system that satisfied the criteria in Table 1 and matured between 0–70°N and 70–160°E was recorded by the software. This large spatial domain covers most parts of AWPR.

3.1 *Data*

The infrared satellite data provided by Kochi

University in Japan was from three geostationary satellites: GMS5 (Geostationary Meteorological Satellite 5), GOES9 (Geostationary Operational Environment Satellite 9) and MTSAT-1R (Multi-functional Transport Satellite 1R). The temporal resolution of the data was 1 h. For each year from 1996 to 2008, the data was available for the range of May through October. For the year 1995, however, only the data of September and October was available. Therefore, the data was of 80 months with time levels added up to 58,872. Occasionally, there were missing data (most notably in May 1999, July and August 2005), but overall it was a consistent dataset that provided fundamental information about each of the MCSs. The spatial resolution of the grid data was 0.05 degree in both the meridional and zonal directions. It is important to note that, unlike the GMS5 and MTSAT-1R which were located in 140°E, GOES9 was located in 155°E. Then, the GOES9 data would not be precise enough in 70–80°E as a result of the edge effect. Hence, the data of GOES9 (from May 22 to July 14, 2005) in 70–80°E was not processed in the present study.

3.2 *Automatic MCS identification method*

The original data used in this study was the infrared satellite gray data interpolated on a 0.05°×0.05° grid. The gray data was then inverted to brightness temperature data after calibration. And then, the AMI method was used, in three steps, to sample MCSs from the grid data. The first step was to search, compute and save all the potential MCS profiles on every cloud picture. The second was to track the potential MCS from its initial profile and the third was to determine if the system found in step 2 was a MCS or not according to the definitions in Table 1.

However, it is important to mention that some TCs and a few cirruses may be included in the MCS database after the three steps of the AMI method. TCs have a high cloud top, the temperature of which is often below –52°C. In addition, the temporal and spatial size of TCs is always large enough to meet the MCS criteria in Table 1. Therefore, we should remove TCs from the MCS database based on TC annuals. According to the studied areas in the present work, the *CMA-STI tropical cyclone best track data set*, provided by China Typhoon Network (http://www.typhoon.gov.cn), and the *Northern Indian Ocean tropical cyclone best track data set*, provided by Joint Typhoon Warning Center (JTWC), were used to remove TCs in the western Pacific region and the northern Indian Ocean region, respectively. The process of removing TCs from the database is somewhat subjective, and the preceding squall lines in association with TCs were also removed from the MCS database. As far as cirruses are concerned, the study by Yu and Chen[24] indicated that the cirrus is hard to have a cloud top temperature below –52°C and more difficult to meet the MCS criteria. Thus, there is no need to remove cirruses from the MCS database in the present work. The study by Shu and Pan[12] pointed out that, the missing and wrong rate of MCS numbers with the AMI method was lower than 2% after removing TCs, and cases of wrong identification caused by cirruses were infrequent. The accuracy of capturing the whole MCS lifecycle by the AMI method could reach about 85%, and the main factor that affected the accuracy was the combination and abruption of the system.

4 RESULTS AND MCS CHARACTERISTICS

By means of the infrared satellite numerical data, the AMI method was used to sample the MCSs over AWPR during the warm seasons of 1995 to 2008. After eliminating the TCs according to the TC annuals, 47468 MCSs were identified. Based on this database, MCS characteristics such as shape, size, duration, velocity, geographical distribution, intermonthly variation, and lifecycle were studied. Results are shown in Table 2. Major axis is defined as the longest line segment with its two endpoints on the MCS profile; minor axis is defined as the line segment perpendicular to the major axis, and the two endpoints of the minor axis must be on the MCS profile; eccentricity is defined as the ratio between the minor axis and major axis; duration is defined as the time lasting from formation to dissipation. Table 2 shows that MαECSs are the most common MCS. Linear MCSs (MECS) are 2.5 times the number of circular MCSs (MCCS), and larger MCSs (MαCS) are 2.5 times the number of smaller MCSs (MβCS). Similar to the situations of MCSs over the U.S.A.[4], the spatial size of the MECS is a little larger than the MCCS in AWPR. As far as the eccentricity is concerned, the means and standard deviations of MαCS and MβCS are almost the same. The MαCS has a much longer duration than the MβCS, though it has the same duration criterion, i.e. 3 h in Table 1. Moreover, the duration of the MCCS is a little longer than that of the MECS.

Table 2. Statistics for MCSs over AWPR during 1995–2008: Means and standard deviations.

Category	Number	Maximum area (km^2)	Length of major axis (km)	Eccentricity	Duration (min.)
MαCCS	9,241	157,502(107,553)	679(254)	0.632(0.097)	446(287)
MβCCS	3,981	72,516(31,591)	470(123)	0.625(0.096)	258(103)
MαECS	25,126	186,424(128,860)	918(352)	0.346(0.084)	416(271)
MβECS	9,120	75,955(34,527)	596(166)	0.344(0.084)	248(94)

Note: The length of major axis and eccentricity were calculated when MCSs reached the maximum extent.

4.1 *Basic characteristics from infrared satellite imagery: shape, size, and duration*

Figures 1a and 1b provide the distributions of eccentricity for MαCS and MβCS in AWPR, respectively. The average eccentricities for MαCS and MβCS were 0.423 and 0.429, respectively. Note the distribution curves for both the larger and smaller MCS classifications. It is found that MαCS and MβCS have similar MCS distributions, i.e. there are no relations between the shape and area of MCSs. Most of the MCSs fit into the eccentricity interval 0.25–0.45. MCSs with eccentricities less than 0.5 (i.e. MECSs) take on an indention distribution, while the number of MCCSs decreases rapidly with the eccentricity increasing. Quasi-circular MCSs with eccentricities more than 0.9 are infrequent. Since Maddox[5] used 0.7 as the eccentricity criterion to define the MCC in North America, many researchers followed to use 0.7 to define circular MCSs. But, as shown in Table 1, 0.5 was used as the eccentricity threshold in this study, which goes with the meaning of Figure 1. This eccentricity threshold (i.e. 0.5) differentiates the indention distribution from the exponential decline distribution. Using 0.5 as the eccentricity threshold corresponds with the MCS characteristics of shape in AWPR.

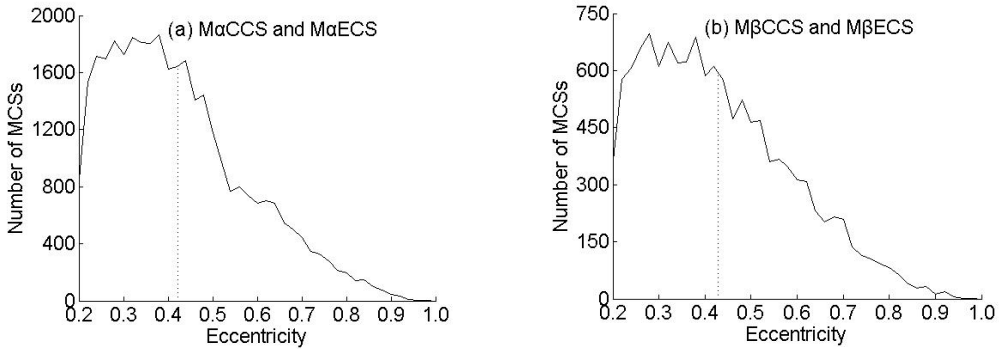

Figure 1. Distributions of different MCS categories as a function of eccentricity (calculated when MCSs reached the maximum extent; curves show the distributions; the point of intersection between the vertical dashed line and the *x* axis denotes the mean value).

Figure 2 provides the distribution curves of AWPR MCSs as a function of size. The upper panel displays the distributions as a function of area; the lower panel displays the distributions as a function of length of the major axis. The left panel displays the distributions of circular MCSs; the right panel displays the distributions of elongated MCSs. Examination of the figure reveals that the number of both circular and elongated MCSs decreases exponentially with their areas growing, which supports the general expectation of an exponential decrease in the number of MCSs when their duration increase (Cotton et al.[25]). But, it seems contrary to the fact in Table 2 that more systems fit into the larger MCS classifications than the smaller MCS classifications. In fact, that is due to the nature of the MCS definitions used in this study. There are both a lower size limit and an upper size limit for MβCS, but there is not an analogous upper size limit for MαCS. As a result, more systems fall into the larger MCS classifications even though smaller systems are actually more common, as seen in Figure 2. In addition, it is noteworthy that the distribution curve for MECS decreases more slowly than MCCS when their duration increase, i.e. there are more chances for MECS to have a larger area. As far as the distributions of the length of the major axis are concerned, they are both single peak distributions for MCCS and MECS. MCCS and MECS have a peak frequency at about 450 km and 550 km, respectively. The length of the major

axis for MCCS and MECS are mainly distributed in 400–800 km and 500–1,100 km, respectively. MCSs rarely have a major axis longer than 2,000 km, which is just the expected upper limit of mesoscale weather systems by Orlanski[13].

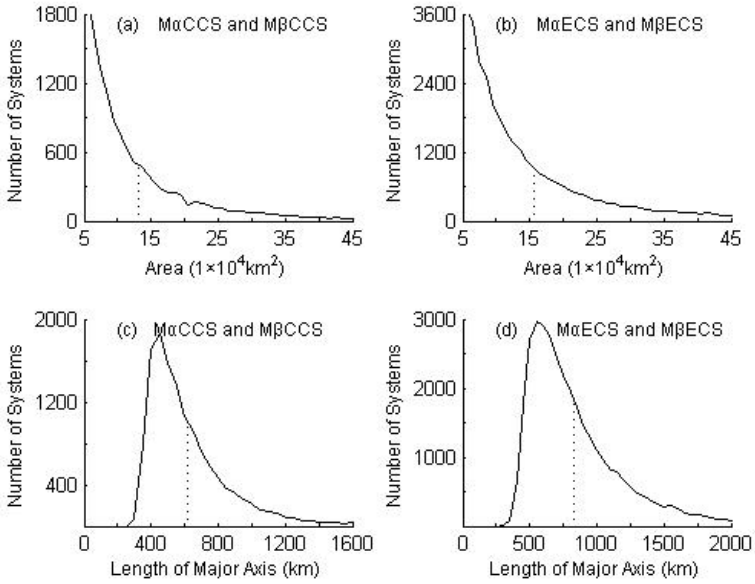

Figure 2. Distributions of different MCS categories as a function of area or length of major axis. Captions are the same as Figure 1.

Figure 3 provides the distribution curves of AWPR MCSs as a function of duration, in which panels a, b, c and d correspond to the situations of M*α*CCS, M*β*CCS, M*α*ECS and M*β*ECS, respectively. Clearly, the distributions of four different MCS categories are similar. The number of systems decreases exponentially when their duration increase. Comparison of panels a, b, c and d indicates that the duration for M*α*CS is much longer than M*β*CS, though there is little difference between MCCS and MECS. It means that the main impact factor for MCS durations is the area of MCS, and shape has little influence on MCS durations. Further analysis on the mean durations of the four categories finds that, in AWPR, the mean durations of M*α*CCS (7.43 h) and M*β*CCS (4.3 h) are only a little longer than those of M*α*ECS (6.93 h) and M*β*ECS (4.13 h), respectively.

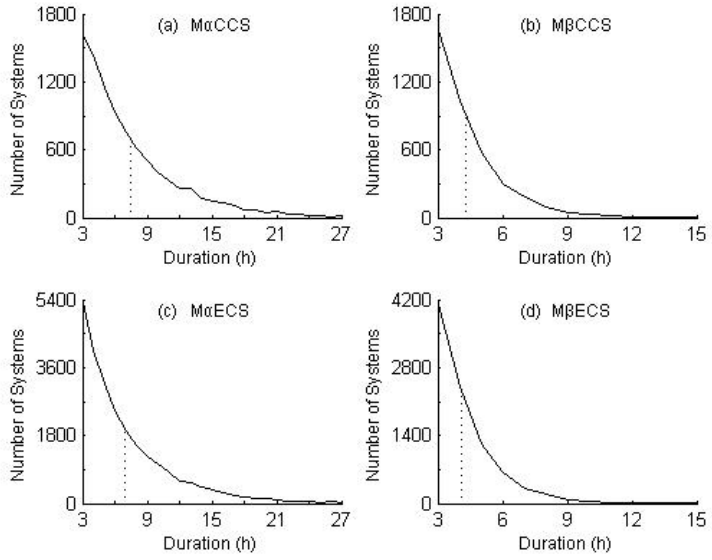

Figure 3. Distributions of different MCS categories as a function of duration. Captions are the same as Figure 1.

4.2 *Velocity characteristics*

Firstly, it is important to keep in mind that both the MCS velocity mentioned in this section and the characteristics of temporal-spatial distribution mentioned in the following sections were analyzed with the MCS cold cloud shield. The MCS velocity denotes the velocity of the centroid of the cold cloud shield. Speed is got from the division of spherical distance by time, and the direction is pointed from the position of centroid of the former time to the latter time. The MCS movement is influenced by many factors, mainly including environmental factors (i.e. external factors, such as the vertical distribution and vertical shear of the wind, and the distribution of the potential instability stratification) and internal factors (such as the size, intensity, and evolvement of the system). The environment flow can lead the movement of the system, the propagation of convective cells and clusters will bring on a shift of the system, and the rotary convective cells will shift left or right as a result of the Magnus force. Under the above factors, the movement of MCSs becomes quite complicated.

MCSs are well-developed convective systems, the top of which can often reach the tropopause. Thus, the steering flow of MCS is the average air flow of the whole troposphere. Approximately, the 500 hPa air flow can be used as the steering flow of MCSs[26]. To find some useful cues to the steering flow, the average 500 hPa wind field in AWPR during the warm seasons of 1995 to 2008 was plotted (figure omitted due to limited space). From the figure, it is found that 23°N is the boundary between the easterlies and westerlies. Hence, to study MCS characteristics of velocity under different steering flows, MCSs are divided into two categories by 23°N. MCSs with the position of centroid lying to the south of 23°N are classified as low latitude MCS, and the rest of the MCSs are classified as mid-high latitude MCS. Furthermore, the MCS velocity is divided into the velocity before maturation and after maturation. The velocity before maturation is calculated by the positions of formation and maturation, while the velocity after maturation is calculated by the positions of maturation and dissipation. Therefore, after calculating from the MCS database, low latitude MCSs have the average speed at about 43.0 km/h and 53.7 km/h before and after maturation, respectively, while mid-high latitude MCSs have the average speed at about 50.2 km/h and 55.5 km/h before and after maturation, respectively. The results indicate that the speed of MCS is close to the speed of the steering flow. Mid-high latitude MCSs move faster than low latitude MCSs due to the faster steering flow. In addition, all MCSs have a propensity to move faster after maturation.

Figure 4 provides the distributions of MCS velocity. The abscissa and ordinate denote the zonal speed and meridional speed of the system, respectively. Thus, the connecting line from the origin of coordinates to any point in the coordinate plane stands for the velocity vector. Shade denotes the number of systems with a corresponding velocity. Figure 4 shows that the MCS velocity is in an elliptical ring shaped distribution on the whole, but the center of the ellipse shifts away from the origin of coordinates. Comparing Figures 4a with 4b, the speed of low latitude MCSs rarely exceeds 60 km/h before maturation but systems speed up after maturation, and more systems distribute in the outside of coordinates. Affected by the easterlies steering flow, more systems move to the west than to the east, and most of the low latitude MCSs move slowly to the west at about less than 30 km/h. However, there is a part of low latitude MCSs moving to the east, because in the easterlies some systems were controlled by the west-steering flows. On the other hand, both the distribution of the potential instability stratification and internal evolvement of the system could result in a movement opposite to the steering flow. Comparing Figures 4c with 4d, mid-high latitude MCSs move a little faster after maturation. Affected by the westerlies steering flow, most of mid-high latitude MCSs move to the east slowly at about less than 30 km/h. As expected, there are a small part of mid-high latitude MCSs moving to the west, reasons of which are the same as the east-moving low latitude MCS.

4.3 *Characteristics of geographical distribution*

By means of the MCS database, MCS numbers of every grid point of the geographical coordinate are counted. A 5°×5° rectangular box with the grid point as the center is used to restrict the counting area. The results are shown in Figure 5. The geographical distributions of the four categories are similar on the whole, but there is much difference in the frequency. MαECS and MβCCS have the highest and lowest frequency, respectively. It is notable in Figure 5 that the distribution of MCSs is related to the latitude directly. MCS activities are mainly concentrated in the mid-low latitude areas. MCSs are in zonal distribution, with three zones weakening from south to north. The low-latitude zone lies south of 25°N, the mid-latitude zone between 25–38°N, and the high latitude zone north of 38°N. Due to the differences in topographic distribution, sea-land distribution and climatic environment, MCS activities could be entirely different even in the same zone.

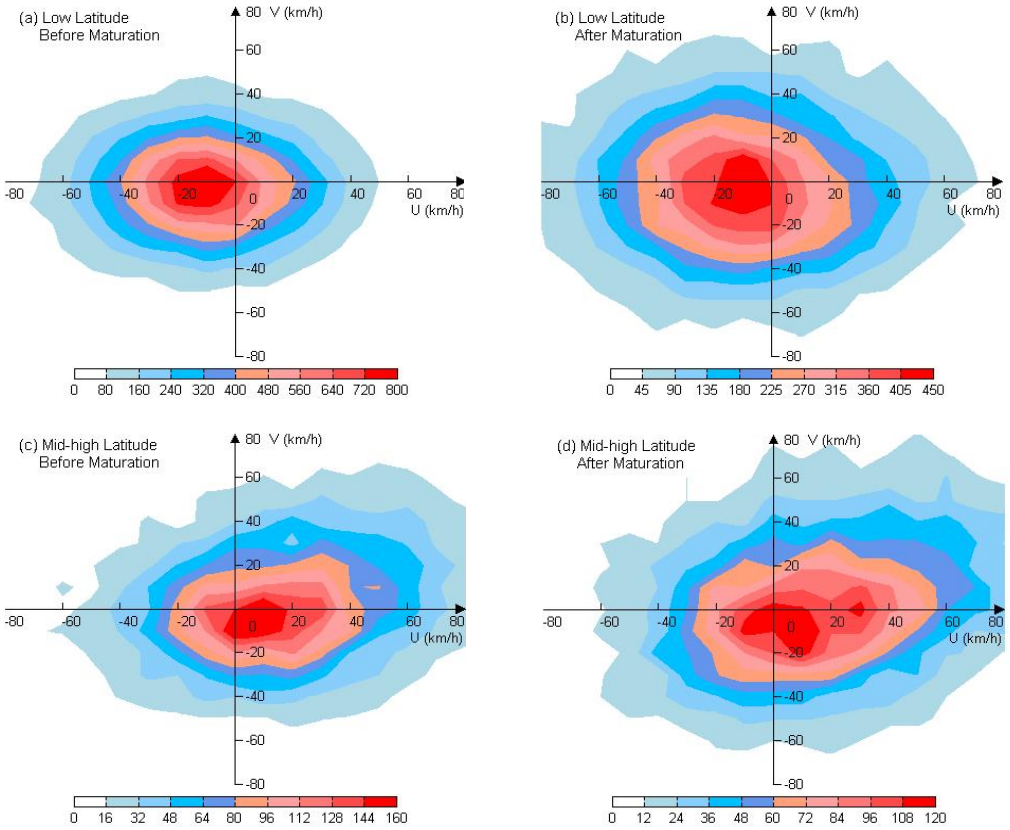

Figure 4. Distributions of MCS velocities. (a): distribution of low-latitude MCSs before maturation; (b): distribution of low-latitude MCSs after maturation; (c): distribution of mid-high latitude MCSs before maturation; (d): distribution of mid-high latitude MCSs after maturation. Axes: speed of the systems; shade: number of systems.

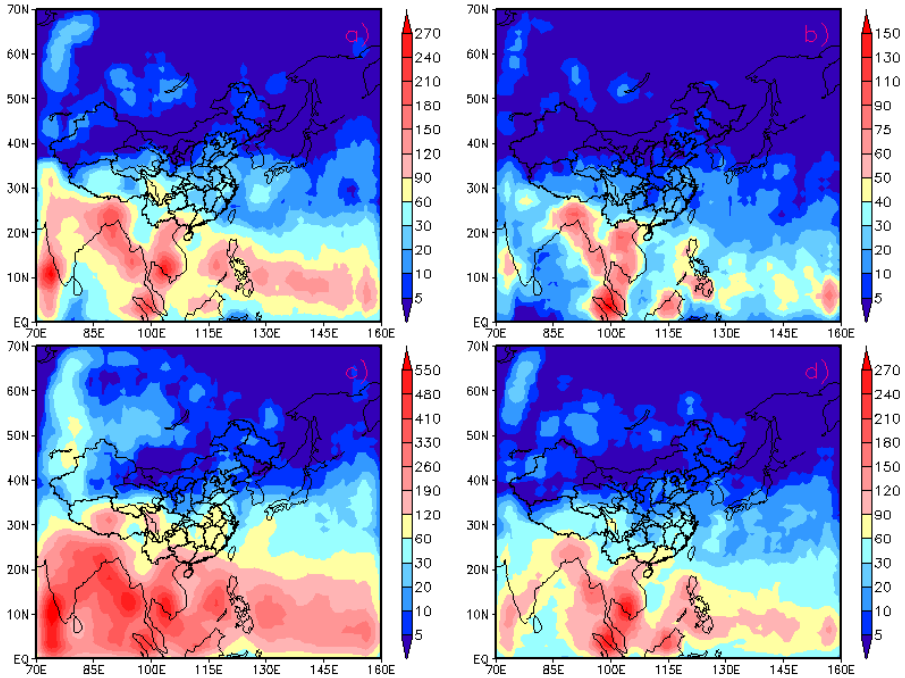

Figure 5. Geographical distributions of four MCS categories. ((a), (b), (c) and (d) correspond to M αCCS, M βCCS. M αECS and M βECS, respectively. Shades: number of systems. MCSs are counted according to their positions when they reach maximum extent.

MCSs in the low latitude zone mainly distribute in the Amindivi and Laccadive Islands regions to the southwest of the Indian Peninsula, Pakistan and Gangetic Plain region, eastern Bay of Bengal, Strait of Malacca, Indochina Peninsula, South China Sea region west of the Philippines, and Caroline Islands region east of the Philippines. This active zone is primarily related to the Inter-Tropical Convergence Zone (ITCZ). Every year, the ITCZ swings between 5–20°N during the warm season. Therefore, the low-latitude area is in a strong low-level convergence and has remarkable upward motion the whole summer. In addition, because the oceans account for a large portion of the area, the low levels of this area are of high temperature and humidity, which result in a marked convective instability. Such kind of large-scale environment is responsible for the high frequency of MCSs in this area. The South Asian Summer Monsoon (SASM) and low-level jet (LLJ) bring sufficient vapor, heat, and momentum to the areas around the Bay of Bengal and Arabian Sea, which is beneficial for producing strong potential instability stratification. Besides, both the vapor and mass convergence in front of the jet maxima and the positive vorticity area on the left of jet stream axis are helpful for continuing development of severe convective systems. With the up-building of the South Asian High in summer, the Indian monsoon region is in a divergence field in the upper levels, which could take away the mass and heat near the top of the convective cloud and is conducive to the upward motion as well as the maintenance of potential instability. Such kind of circulation configuration of upper and lower levels make MCS activities more active in the Indian monsoon region than in the areas east and west of the Philippines. Due to favorable environment, the larger systems account for a dominant portion west of 85°E in low-latitude zones. Besides, it is noticeable in the Indian monsoon region that the terrain plays an important role in MCS distribution. The MCS active centers are located in the low-altitude side of the area of transition between high and low altitudes, such as the Arabian Sea on the windward side of Western Ghats Mountain Range, Pakistan and Gangetic Plain to the south of the Himalayas, Bay of Bengal to the west of the Arakan Mountains, and the lower Mekong River plain. Blocking of the high terrain is helpful for the persistent upward motion and vapor convergence, which is responsible for the frequent convective activities in these low-altitude areas. Finally, it is found in Figure 5 that there are some MCS activities south of 5°N. It means that different from TCs, the β-effect is not necessary in MCS formation.

MCSs in the mid-latitude zone mainly distribute in the north of the Indus Plain, central and western part of the Tibetan Plateau, Hengduan Mountains region, Sichuan Basin, east of China, and oceans near the Ryukyu Islands. One remarkable characteristic of this zone is that the active and inactive centers are alternated, and it is even more prominent for MαCCS. This result agrees with the conclusion by Zheng et al.[23]. MCSs in the Hengduan Mountains region and the north of the Indus Plain are associated with the upward motion caused by the terrain block of the SASM from the Arabian Sea and Bay of Bengal. It is noteworthy that circular MCSs account for a large portion in the north of the Indus Plain. MCSs in the Tibetan Plateau are related to the thermal effect of the plateau. In summer, the tropical depression occupies the low levels, and there are strong current convergence and upward motion in the depression. Due to the pyrogenic effect of the plateau, the atmosphere on the plateau presents convective instability. Thus, the particular geographical environment of the Tibetan Plateau gestates the convective systems. MCSs in the Sichuan Basin are related to the particular topographic condition and mountain-valley breeze. MCSs in the east of China and oceans near the Ryukyu Islands are associated with the East Asian Summer Monsoon (EASM) and Meiyu front, and the Kuroshio Current as well as the TC activities are also important reasons for the high frequency in the vicinity of Ryukyu Islands. Over the ocean to the east of Japan, the North Pacific Current and East Asia major trough provide favorable conditions for convective activities.

There are only a few MCS activities in the high latitude zone, the comparatively active regions of which include the central part of the West Siberian Plain, Lake Balkhash and Lake Issyk-Kul areas north of the Tianshan Mountains, Sayan Mountains and Lake Baikal areas north of Mongolia, and areas on the east of Great Khingan Mountains. Except the regions mentioned above, the rest of the zone is inactive for MCSs. The low frequency in this zone is due to the fact that the summer monsoon could hardly reach these high-latitude areas and the temperature of the land surface and sea surface in this zone are quite low. The comparatively active regions are related to some high-latitude weather systems. For instance, a trough of low pressure often occurs to the west of the Ural Mountains in winter, which might cause the convective activities in the central part of the West Siberian Plain that is in front of the trough. MCSs in the north of the Tianshan Mountains are associated with the Tianshan quasi-stationary front, and many lakes in this area could provide favorable vapor conditions for MCS development.

4.4 *Characteristics of intermonthly variation*

Due to different geographical locations, MCSs in

different regions are expected to have different intermonthly variation characteristics. The tropic of cancer was used to divide MCSs into two types: low-latitude MCSs and mid-high latitude MCSs. Figure 6 provides a breakdown of MCS frequency for each of the 6 months during the 14-yr period. Figures 6a and 6b correspond to mid-high latitude MCSs and low-latitude MCSs, respectively. Due to the data used in this study, the MCS numbers for September and October in Figure 6 are multiplied by 13/14. Figure 6 shows that, four MCS categories have similar characteristics of intermonthly variation in both the mid-high latitudes and low latitudes. However, all MCSs in mid-high and low latitudes have distinct intermonthly variation characteristics from each other. For mid-high latitude MCSs, July has the largest chance for MCS to occur, August comes second, and both September and October are the least likely months for MCSs to develop. While for low-latitude MCSs, June, July, August, September and October have about equal chances for MCS occurrence; and May has fewer MCS activities than other months. The results are as expected. Every year the subsolar point moves between the tropics, which means that monthly variation should have less influence on low-latitude MCSs than mid-high latitude MCSs.

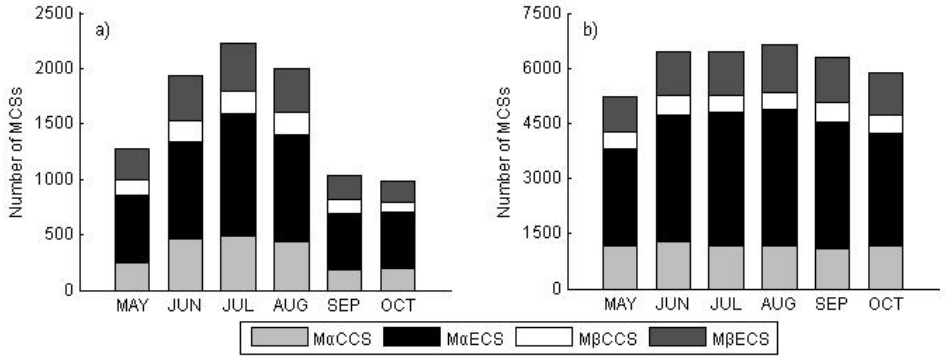

Figure 6. Distributions of four MCS categories by month. (a): mid-high latitude MCSs; (b): low-latitude MCSs.

Figure 7 provides the geographical distributions of four MCS categories by month during the 14-year period. The numbers of systems in September and October are also revised by 13/14. Figure 7 shows that affected by different climatic and geographical environment, MCSs in different regions have different intermonthly variation characteristics; however, in a certain region, intermonthly variation characteristics of the four MCS categories are similar to each other. Hence, in the following the entire MCSs are used as a sample to study the intermonthly variation characteristics in detail.

Figure 8 provides the geographical distributions of all MCSs by month, with September and October revised similarly. The intermonthly variation characteristics are analyzed in detail by region as follows. MCSs in the Indian monsoon region are mainly influenced by both the advance and retreat of SASM and the location of the Indian Monsoon Trough (IMT). In May, the IMT is more southward than in other months of the warm season, so active MCS centers are also distributed more southward. With the SASM onset and advancing northward in June, active MCS centers also advance northward to about 30°N. MCSs in the Arabian Sea, Bay of Bengal, Indian Peninsula and Indochina Peninsula are quite active. When it comes to July, the SASM arrived at the northernmost location of the year, and the active MCS centers in the Indian monsoon region also advance to the northernmost location. From August on, these centers keep on retreating southward with the SASM retreating southward. MCSs in the southwest and south of China, including Guangdong and Guangxi, the northeastern part of Yunnan-Guizhou Plateau and Hengduan Mountains, are also related to the SASM. In May, there are already some MCS activities in this region. And the convective activities have a peak frequency in June and July, with August coming next. Though, there are few systems in this region in September and October, MCS activities in the Tibetan Plateau have a peak frequency in July and August, and there are fewer systems in other months. From October on, MCSs rarely occur over the plateau. In July and August, the SASM jumps on the plateau, the South Asia high occupies the high levels of the plateau, and the thermal effect of the plateau is intense in the two months. Acting together, these beneficial factors cause the high frequency of MCS.

Intermonthly variation of MCSs over the South China Sea region and Caroline Islands region is related to the advance and retreat of the ITCZ as well as western Pacific subtropical high (WPSH). Figure 8 shows that, the active MCS center in this region is nearly the location of the ITCZ, and the northern extremity of this active area is on the south of the WPSH. In May, the ITCZ and WPSH lie more southward, and the active MCS area is to the south of 10°N. With the WPSH and ITCZ moving northwards in June, the active MCS area expands to about 13°N.

By the middle of July, the ITCZ, WPSH and active MCS area have been expanding northwards together. The WPSH arrives at the northernmost location in August and then remains steady for a few days, while the ITCZ reaches the northernmost location in early September. Hence, the active MCS area expands to the northernmost location in August, and the northern extremity of this area maintains at about 20°N. In September and October, the active area retreats southward with the ITCZ and WPSH.

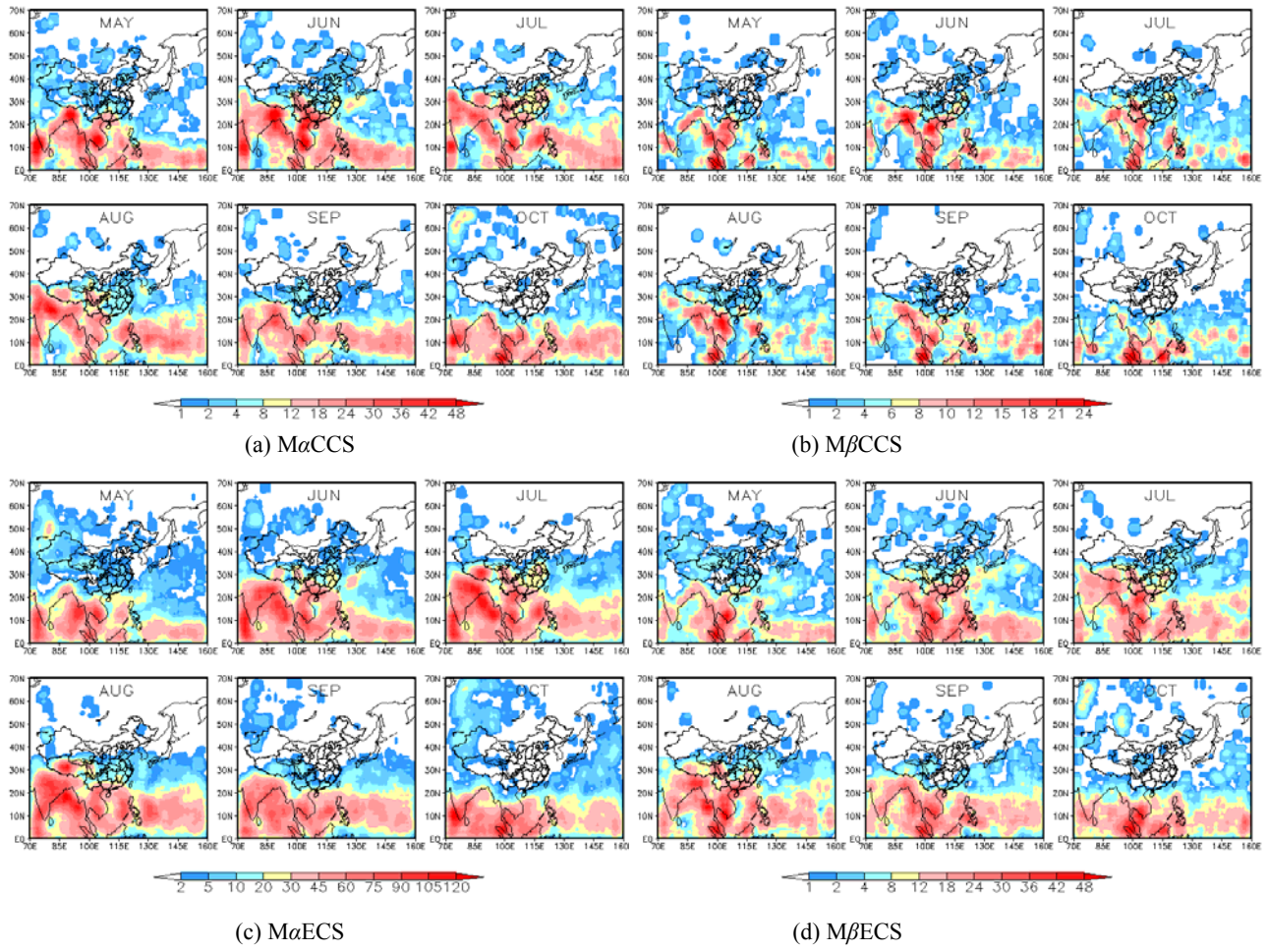

(a) MαCCS (b) MβCCS

(c) MαECS (d) MβECS

Figure 7. Geographical distributions of the four MCS categories by month. (a): MαCCS; (b): MβCCS; (c): MαECS; (d): MβECS. Other captions are the same as in Figure 5.

Intermonthly variation of MCSs in the middle and lower reaches of the Yangtze River, Huanghuai Plain, southeast coast of China, and oceans near the Ryukyu Islands is mostly related to the EASM, the quasi-stationary front and WPSH. In May, the subtropical ridgeline lies at about 17°N. The EASM and cold air from the north form a quasi-stationary front in south China, and cause convective activities as well as continuous precipitation. By the middle of June, the subtropical ridgeline has jumped over 20°N. The EASM and cold air from the north form the Meiyu front in the Yangtze-Huaihe region and Ryukyu Islands region. Affected by the Meiyu front, MCS activities are frequent in the two regions. With the subtropical ridgeline jumping northward again in the middle of July, the Meiyu front and active MCS area move northward to the Huanghuai Plain. Generally speaking, the active MCS area is expanding along with the expansion of the EASM. From August on, the EASM, WPSH and active MCS area retreat southward together. In August, there are still some MCS activities in both the middle and lower reaches of the Yangtze River and the Ryukyu Islands region. In September and October, however, MCSs rarely occur in these regions. When it comes to October, the MCS distributing belt retreats from the mainland of China.

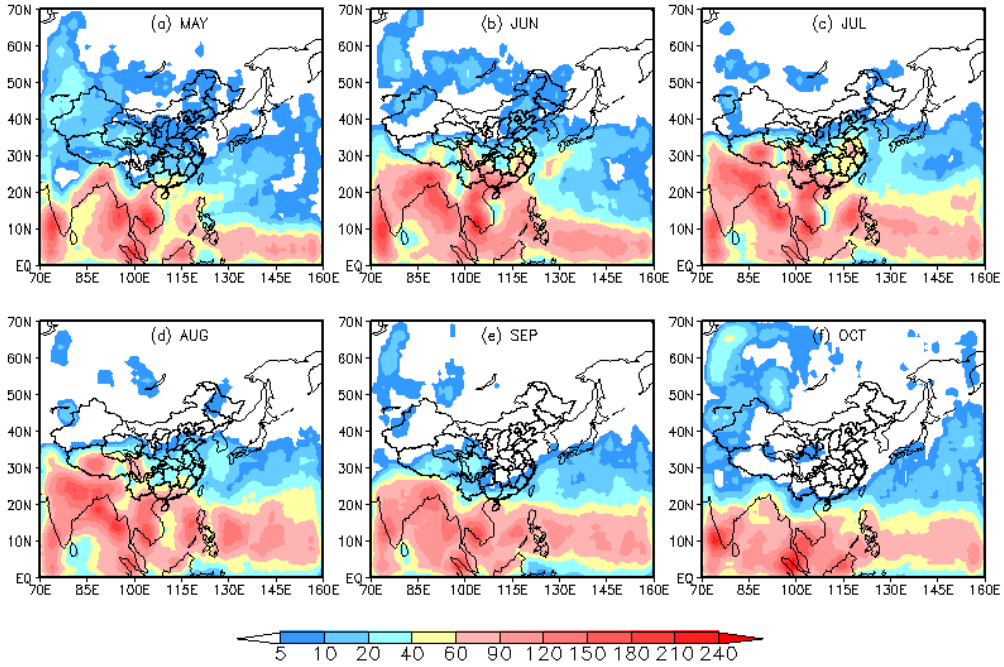

Figure 8. Geographical distributions of all MCSs by month. Other captions are the same as in Figure 5.

On the north of 38°N, because the ground surface temperature is low and the summer monsoon could hardly reach, MCSs are inactive over there during the warm season. Occurrences of MCS in this region are mainly related to the mid-high latitude weather systems, and the intermonthly variation is associated with the seasonal adjustment of westerly troughs and ridges. Examination of Figure 8 reveals that MCS frequency continually decreases in the northern areas from May to August, which corresponds to the long-wave adjustment of the 500 hPa troughs and ridges. During the transition of large scale circulation from winter to summer, the trough activities in the northern areas decrease, being unfavorable for MCS activity. In September, the large scale circulation begins to adjust towards the winter situation, the European shallow trough in the vicinity of Ural Mountains and the ridge of high pressure in the Lake Baikal region begin to establish. Thus, MCS activities in the areas west of 105°E, where it is in front of the trough and behind the ridge, begin to increase; however, the northeast China, which is in front of the Lake Baikal ridge, rarely has any MCS activities. In October, with the up-building of East Asia major trough near 140°E, MCSs begin to occur over Kamchatka Peninsula and the oceans east off Japan, where they are in front of the major trough.

The following is a summary for what is described above. Four satellite-defined MCS categories in the same region have similar characteristics of intermonthly variation, and the intermonthly variation is mainly influenced by both the climate environment and geographical environment. Intermonthly variation of MCSs in the Indian monsoon region, south China, and Tibetan Plateau region is mainly influenced by both the advance and retreat of SASM and the location of the IMT. MCSs in the South China Sea region and western Pacific region east of the Philippines are closely related to the advance and retreat of the ITCZ and WPSH; MCSs in the middle and lower reaches of the Yangtze River, Huanghuai Plain, southeast coast of China, and oceans near the Ryukyu Islands are mostly related to the EASM, quasi-stationary fronts and WPSH. Intermonthly variation of MCSs north of 38°N is related to the seasonal adjustment of westerly troughs and ridges. In addition, intermonthly variation of MCSs is possibly affected by the topographic distribution. For instance, the strong thermal effect of the Tibetan Plateau in July and August causes the high frequency of MCSs over the plateau in the two months.

4.5 *Lifecycle characteristics of MCSs in China*

To study in detail the lifecycle (i.e. formation, maturation and dissipation) characteristics of MCSs over different underlying surface in China, the following nine areas which have typical underlying surfaces are chosen:

(a) Tibetan Plateau, 80–100°E, 30–35°N,

(b) Yunnan-Guizhou Plateau, 99–105°E, 23–28°N,

(c) Hilly areas in the southeast of China, 117–120°E, 27–30°N,

(d) Huanghuai Plain, 114–120°E, 32–35°N,

(e) Northeast Plain, 122–127°E, 43–48°N,

(f) Sichuan Basin, 103.5–106.5°E, 28.8–31.5°N,

(g) Coastal areas of Guangdong and Guangxi, 108–113°E, 22–23°N,

(h) East China Sea, 123–128°E, 26.5–32.5°N, and

(i) South China Sea, 112–120°E, 12–20°N.

By means of the MCSs which matured in the nine areas, Figure 9 and Table 3 are plotted. Figure 9 provides the lifecycle curves in these areas and Table 3 presents the statistics.

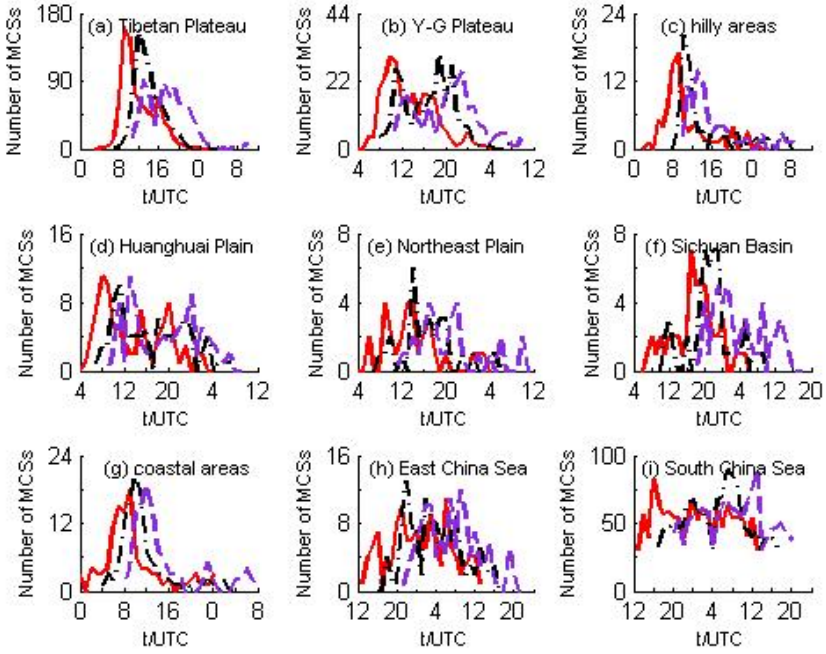

Figure 9. Lifecycle curves of MCSs over the nine areas of China. (The solid red line, dash and dot black line, and dashed purple line denote the formation, maturation and dissipation, respectively)

Table 3. Mean values for MCSs in the nine areas of China from 1995 to 2008. (Area and eccentricity correspond to the time when MCSs reach the maximum extent)

Region	Total number of systems				Time (UTC)			Duration (h)	Area (10^3km^2)	Eccentricity
	MαCCS	MβCCS	MαECS	MβECS	Formation	Maximum	Dissipation			
(a)Tibetan Plateau	134	56	495	147	11:47	13:49	17:23	5.6	198	0.399
(b)Y-G Plateau	66	25	108	49	12:28	16:07	19:40	7.2	123	0.453
(c)Southeast hilly areas	16	4	42	20	10:20	12:46	14:59	4.6	111	0.429
(d)Huanghuai Plain	16	10	54	9	12:27	15:40	18:51	6.4	122	0.433
(e)Northeast Plain	7	7	9	7	11:46	14:24	16:34	4.8	84	0.477
(f)Sichuan Basin	17	4	23	7	14:50	18:06	21:38	6.8	113	0.463
(g)Coastal areas	24	8	44	31	08:58	11:40	14:33	5.6	117	0.413
(h)East China Sea	25	17	57	24	11:21	14:46	18:04	6.7	110	0.452
(i)South China Sea	258	97	722	205	11:25	15:17	18:53	7.5	162	0.430

Figures 9a and 9b show that MCSs in plateau areas have only one peak in their lifecycle curves. They mostly form at about 3 pm local time, develop for several hours, mature at nightfall and dissipate at

night. As can be seen from Table 3 that, average duration for MCSs in Tibetan Plateau and Yunnan-Guizhou Plateau are 5.6 h and 7.2 h, respectively. However, the Tibetan Plateau MCSs have a much larger spatial size, and the average maximum area is close to 200,000 km^2. In Tibetan Plateau, linear MCSs account for a large proportion of all MCSs, and the average eccentricity is lower than 0.4. Figure 9c shows that lifecycle curves of MCSs in the hilly areas in the southeast of China are also in a single-peak distribution. MCSs in this region mainly form at about 4 pm local time, and have a relatively short duration and small area. It is found in Figures 9d and 9e that MCSs in plain areas have several peaks in their lifecycle curves and MCSs might form either in the afternoon or at night. From Table 3, Huanghuai Plain MCSs are known to have a larger temporal and spatial size than Northeast Plain MCSs. Due to the high latitude, the environment in the Northeast Plain is unfavorable for MCS development. As a result, many systems in this area develop into the smaller MCSs. In addition, circular MCSs here account for a relatively large proportion. It is eye-catching in Figure 9f that most of the MCSs in Sichuan Basin occur nocturnally. Affected by the local mountain-valley breeze circulation, the upward motion in the basin at night is favorable for convective activities. MCSs in this area mainly form at about 1 am midnight, mature in the early morning and dissipate in the daytime, with average duration at 6.8 h. Figure 9g shows that lifecycle curves of MCSs in coastal areas of Guangdong and Guangxi are also in a single-peak distribution, and most of the systems form at about 3 or 4 pm, mature at nightfall and dissipate at night. The sea-land breeze circulation is responsible for the lifecycle in this area. In the afternoon, because of the growing temperature on the land and the plentiful vapor brought by the sea breeze, convective activities are intense. Figures 9h and 9i correspond to MCSs in the East China Sea and South China Sea, respectively. The East China Sea MCSs have several peaks in their lifecycle curves, and the largest two peaks for MCS formation are 4 am and 2 pm. Averagely, MCSs in this area can last about 6.7 h (see Table 3). In the South China Sea, due to the favorable large scale environment, the number of MCSs is quite large and the systems are active all day, though midnight (local time) is more likely for MCS occurrence. The temporal and spatial size of MCSs in this area is relatively large. On average, the duration is 7.5 h and the maximum area reaches 162,000 km^2 (see Table 3). In a word, such laws are discovered from Figure 9: MCSs over plateau and hill areas have only one peak in their lifecycle curves and tend to form at about 3 or 4 pm local time; MCSs over plain areas have several peaks in their lifecycle curves; affected by mountain-valley breeze circulation, MCSs in Sichuan Basin occur nocturnally; affected by sea-land breeze circulation, MCSs in coastal areas of Guangdong and Guangxi mainly form in the afternoon; in the night, the relatively high sea surface temperature is responsible for the nocturnal forming peak of the ocean MCSs.

5 SUMMARY AND CONCLUSIONS

In this study, the AMI method and infrared satellite numerical data were used to sample the four categories of MCS over AWPR during the warm seasons of 1995–2008. 47,468 systems were found to meet the MCS requirements. From this database, MCS characteristics such as shape, size, duration, velocity, geographical distribution, intermonthly variation, and lifecycle were studied. The main results are as follows:

(1) MαECS is found to be the most common MCS category. MαCSs are 2.5 times the number of MβCSs, while MECSs are 2.5 times the number of MCCSs. The linear systems are of a larger area, whereas the circular systems are of a longer duration. The eccentricity distributions of MαCS and MβCS are analogous to each other. When the eccentricity is less than 0.5, MCSs takes on an indention distribution; but, when the eccentricity is larger than 0.5, the number of MCSs decreases rapidly with the eccentricity increasing. As far as the size and duration distributions are concerned, the number of MCSs decreases rapidly with the area and duration rising, whereas the major axes are in a single-peak distribution.

(2) The MCS movement is affected by both internal force and external force. The 500 hPa environment flow could be considered as the steering flow for MCSs, and by the action of which, low latitude MCSs tend to move westward and mid-high latitude MCSs tend to move eastward. Generally, mid-high latitude MCSs move faster than low-latitude MCSs, and all MCSs tend to move faster after their maturation. On average, the speed of the low latitude MCS is 43.0 km/h before maturation and 53.7 km/h after maturation, whereas the speed of the mid-high latitude MCS is 50.2 km/h before maturation and 55.5 km/h after maturation.

(3) Four satellite-defined MCS categories have similar characteristics of geographical distribution. In AWPR, MCSs are in zonal distribution, with three zones weakening from south to north. The low-latitude zone lies south of 25°N, the mid-latitude zone lies between 25–38°N, and the high-latitude zone lies north of 38°N. MCSs in the active low-latitude zone are mainly distributed in the Amindivi and Laccadive Islands regions to the southwest of the Indian Peninsula, Pakistan and Gangetic Plain region, oceans in the east of the Bay of Bengal, Strait of Malacca, Indochina Peninsula, South

China Sea region west of the Philippines, and Caroline Islands region east of the Philippines. MCSs in the mid-latitude zone basically distribute in the north of the Indus Plain, central and western part of the Tibetan Plateau, Hengduan Mountains region, Sichuan Basin, east of China, and oceans near the Ryukyu Islands. There are only a few MCS activities in the high latitude zone, the comparatively active regions of which include the central part of the West Siberian Plain, Lake Balkhash and Lake Issyk-Kul areas north of the Tianshan Mountains, Sayan Mountains and Lake Baikal areas north of Mongolia, and areas on the east of Great Khingan Mountains. Generally speaking, the activity of MCSs in a certain region is jointly influenced by the climatic environment, topography distribution and sea-land distribution.

(4) The tropic of cancer is used as the dividing line to study MCS characteristics of intermonthly variation in different regions. As far as the monthly totals for the mid-high latitude MCSs are concerned, July has the largest chance for MCS occurrence; August comes second; September and October are the least likely months for a MCS to develop. While for the low-latitude MCSs, June, July, August, September and October have about equal chances for MCS occurrence; May has fewer MCS activities than other months. Further analysis on characteristics of intermonthly variation in different regions shows that: four satellite-defined MCS categories in the same region have similar characteristics of intermonthly variation; MCS characteristics of intermonthly variation in the Indian monsoon region, South China, and Tibetan Plateau region are mainly influenced by both the advance and retreat of SASM and the location of the IMT; differently, MCS characteristics of intermonthly variation in the South China Sea region west of the Philippines and western Pacific region east of the Philippines are closely related to the advance and retreat of the ITCZ and WPSH; intermonthly variation of MCS activities in the middle and lower reaches of the Yangtze River, Huanghuai Plain, southeast coast of China, and oceans near the Ryukyu Islands is mostly related to the EASM, quasi-stationary front and WPSH; intermonthly variation of MCS activities north of 38°N is related to the seasonal adjustment of westerly troughs and ridges.

(5) The studies on the lifecycle (i.e. formation, maturation, dissipation) curves of MCSs over nine areas of China with different underlying surfaces indicate that: there is only one peak in the lifecycle curves of MCSs in the Tibetan Plateau and Yunnan-Guizhou Plateau, where the systems tend to form in the afternoon, mature at nightfall and dissipate at night; MCSs in the hilly areas in the southeast of China were also of a single-peak lifecycle curve, where most of the systems form at about 4 pm, and the systems there are of a relatively small size and short duration; MCSs over plain areas, which have several peaks in their lifecycle curves, might form either in the afternoon or at night; most of the systems in the Sichuan Basin form at about 1 am midnight, mature in the early morning and dissipate in the daytime; affected by sea-land breeze circulation, MCSs over coastal areas of Guangdong and Guangxi always come into being at about 3 or 4 pm; MCSs in the East China Sea region have several peaks in their lifecycle curves, and the two largest peaks of formation are after midnight and in the afternoon; MCSs in the South China Sea region are alive all day with a formation peak in the midnight.

Different from the study by Zheng et al.[23], this study used the AMI method to get a large MCS sample, in which each MCS is recorded from its formation to dissipation, and conducted research on MCS characteristics such as shape, size, duration, velocity, geographical distribution, intermonthly variation, and lifecycle. The revolutionary method explores an easy, efficient and feasible way for MCS census and makes it possible to do MCS census on a large time and space frame. In future studies, we are going to inquire about the MCSs in other continents with the AMI method. In addition, the AMI method might also be used in operational systems to forecast severe convective systems by means of the cloud-top temperature. Finally, we sincerely hope that this study could aid the forecasters and researchers in gaining a deeper insight into the MCSs over AWPR, as these violent systems could have a great influence on people's livelihood.

Acknowledgement: The authors wish to thank the Atmospheric Department of Kochi University for providing the infrared satellite numerical data.

REFERENCES:

[1] MADDOX R A, ROGERS D M, HOWARD K W. Mesoscale convective complexes over the United States during 1981—An annual summary [J]. Mon. Wea. Rev., 1982, 110: 1501-1514.

[2] HOUZE R A, SMULL B F, DODGE P. Mesoscale organization of springtime rainstorm in Oklahoma [J]. Mon. Wea. Rev., 1990, 118: 613-654.

[3] FRITSCH J M, KANE R J, CHELIUS C R. The contribution of mesoscale convective weather systems to the warm-season precipitation in the Unites States [J]. J. Climate Appl. Meteor., 1986, 25: 1333-1345.

[4] JIRAK I L, COTTON W R, MCANELLY R L. Satellite and radar survey of mesoscale convective system development [J]. Mon. Wea. Rev., 2003, 131(10): 2428-2449.

[5] MADDOX R A. Mesoscale convective complexes [J]. Bull. Amer. Meteor. Soc., 1980, 61(11): 1374-1387.

[6] MADDOX R A. Large-scale meteorological conditions associated with midlatitude mesoscale convective complexes [J]. Mon. Wea. Rev., 1983, 111: 126-140.

[7] MCANELLY R L, COTTON W R. Meso-β scale characteristics of an episode of meso-α scale convective complexes [J]. Mon. Wea. Rev., 1986, 114: 1740-1770.
[8] COTTON W R, LIN M S, MCANELLY R L, et al. A composite model of mesoscale convective complexes [J]. Mon. Wea. Rev., 1989, 117: 765-783.
[9] BLUESTEIN H B, JAIN M H. Formation of mesoscale lines of precipitation: Severe squall lines in Oklahoma during the spring [J]. J. Atmos. Sci., 1985, 42: 1711-1732.
[10] BLUESTEIN H B, MARX G T, JAIN M H. Formation of mesoscale lines of precipitation: Nonsevere squall lines in Oklahoma during the spring [J]. Mon. Wea. Rev., 1987, 115: 2719-2727.
[11] PARKER M D, JOHNSON R H. Organizational modes of midlatitude mesoscale convective systems [J]. Mon. Wea. Rev., 2000, 128: 3413-3436.
[12] SHU Yu, PAN Yi-nong. Self-identification of mesoscale convective system from satellite infrared imagery [J]. J. Nanjing Univ. (Nat. Sci.), 2010, 46(3): 337-348.
[13] ORLANSKI L A. A rational subdivision of scales for atmospheric processes [J]. Bull. Amer. Meteor. Soc., 1975, 56(5): 527-530.
[14] AUGUSTINE J A, HOWARD K W. Mesoscale convective complexes over United States during 1985 [J]. Mon. Wea. Rev., 1988, 116: 686-701.
[15] AUGUSTINE J A, HOWARD K W. Mesoscale convective complexes over United States during 1986 and 1987 [J]. Mon. Wea. Rev., 1991, 119: 1575-1589.
[16] VELASCO L, FRITSCH J M. Mesoscale convective complexes in Americas [J]. J. Geophy. Res., 1987, 192: 9591-9613.
[17] MILLER D, FRITSCH J M. Mesoscale convective complexes in the western Pacific region [J]. Mon. Wea. Rev., 1991, 119: 2978-2992.
[18] LAING A, FRITSCH J M. Mesoscale convective complexes over the India monsoon region [J]. J. Climate, 1993, 6: 911-919.
[19] LAING A, FRITSCH J M. Mesoscale convective complexes in Africa [J]. Mon. Wea. Rev., 1993, 121: 2254-2263.
[20] ANDERSON C J, ARRITT R W. Mesoscale convective complexes and persistent elongated convective systems over the United States during 1992 and 1993 [J]. Mon. Wea. Rev., 1998, 126: 578-599.
[21] MA Yu, WANG Xu, TAO Zu-yu. Geographic distribution and life cycle of mesoscale convective system in China and its vicinity [J]. Prog. Nat. Sci., 1997, 7 (6): 701-706.
[22] ROMATSCHKE U, HOUZE R A. Characteristics of precipitating convective systems in the premonsoon season of South Asia [J]. J. Hydrometeor., (in press).
[23] ZHENG Yong-guang, CHEN Jiong, ZHU Pei-jun. Distribution and diurnal variation of MCS over China and its vicinity in summer [J]. Chin. Sci. Bull., 2008, 53(4): 471-481.
[24] YU Fan, CHEN Wei-ming. Research on the cloud classification for the bi-spectrum cloud picture [J]. J. Nanjing Inst. Meteor., 1994, 17(1): 117-124.
[25] COTTON W R, ALEXANDER G D, HERTENSTEIN R, et al. Cloud venting—A review and some new global annual estimates [J]. Earth-Sci. Rev., 1995, 39: 169-206.
[26] CORFIDI S F, MERRITT J H, FRITSCH J M. Predicting the movement of mesoscale convective complexes [J]. Wea. Forecast., 1996, 11, 41-46.

Citation: SHU Yu, PAN Yi-nong, WANG Wei. Statistic characteristics of MCSs over Asia and western Pacific region. *J. Trop. Meteor.*, 2012, 18(4): 457-472.